Elimination of systematic error in subpixel accuracy centroid estimation

Brian F. Alexander
Kim Chew Ng, MEMBER SPIE
Monash University
Department of Electrical and Computer Systems Engineering
Clayton, Victoria 3168, Australia

Abstract. An analysis of the properties of the centroid method for subpixel accuracy image feature location is presented. This method is free of systematic error if the maximum spatial frequency of the image incident on the image sensor is less than the sensor's sampling frequency. This can be achieved by using a lens aperture setting such that the modulation transfer function cut-off frequency due to diffraction is appropriately small. Both simulation and experimental tests of this prediction are presented for the case of the location of the center lines of the images of projected light stripes in a triangulation-based three-dimensional shape measurement system.

Subject terms: centroid; subpixel accuracy; light stripe location.

Optical Engineering 30(9), 1320-1331 (September 1991).

CONTENTS

1. Introduction
2. Light stripe location using the centroid
3. Systematic error in light stripe location using the centroid
   3.1. Relationship between the centroids of continuous and sampled waveforms
      3.1.1. Two-dimensional centroid
   3.2. Elimination of systematic error in practice
   3.3. Properties of the systematic error
4. Simulations
   4.1. Modulation transfer functions
      4.1.1. Lens MTF
      4.1.2. Image sensor MTF
   4.2. Error versus lens aperture
   4.3. Variation of stripe width
   4.4. Comparison of sensor types
   4.5. Form of the error versus stripe width relationship
      4.5.1. Error versus pixel width relationship
   4.6. Variation of threshold level
5. Experimental results
   5.1. Experimental investigation of systematic centroid error
6. Conclusions
7. Acknowledgment
8. References

1. INTRODUCTION

The centroid method has been widely used for the location of image features of various types to subpixel accuracy.[1–13]

The one-dimensional centroid has been used for light stripe center location in surface measurement systems using active triangulation.[1–5] Its use for edge location by estimation of the center of the peak in the first difference of the pixel values crossing the edge has also been described.[6] The performance of the two-dimensional centroid has been investigated for the location of area targets[7,13] and point sources.[9,10] It has been applied in star trackers.[11,12]

Paper 2915 received May 18, 1990; revised manuscript received Feb. 23, 1991; accepted for publication Feb. 24, 1991.

Two sources of error are usually considered:

1. *Systematic error due to the nature of the algorithm:* This error is reproducible given a particular lens point spread function and a particular position of a particular image feature relative to the array of light sensors.
2. *Error due to noise:* Any deviation in the intensities of the image pixels from the ideal will propagate through to a deviation in the calculated centroid. Some sources of such deviation are shot noise, CCD amplifier noise, CCD pixel response nonuniformity, and quantization noise.

The properties of the systematic error have been investigated with respect to the degree of blur of the image feature[2,7–10] and the width of the sensitive area of the pixels in relation to the pixel pitch.[2,4,8–10] In general, systematic error was reduced by increasing degrees of blur and by the use of pixels of wider sensitive area. However, one result[4] shows error first decreasing and then increasing as pixel width is increased.

In this paper the properties of the systematic error are investigated using a spatial-frequency-based approach. This method will lead to an explanation of the origin of the systematic error and to a method for its removal.

The properties of the error due to noise are described elsewhere[2,8,9,10,13] and are not considered here.

2. LIGHT STRIPE LOCATION USING THE CENTROID

In this paper we study the centroid method in the context of the location of the center lines of an array of projected light stripes used in a triangulation-based three-dimensional surface shape measurement system.[1] The system arrangement is shown in Fig. 1. An array of 64 horizontal light stripes with a mark to space ratio of 1.4:1 is projected onto the surface to be measured using a liquid crystal based white light projector. A camera displaced vertically from the projector views the stripes. After determining the positions and identities of the stripes in the camera's image, the 3-D coordinates of points on the stripes are calculated by triangulation. We achieved coding of the light stripes by pro-

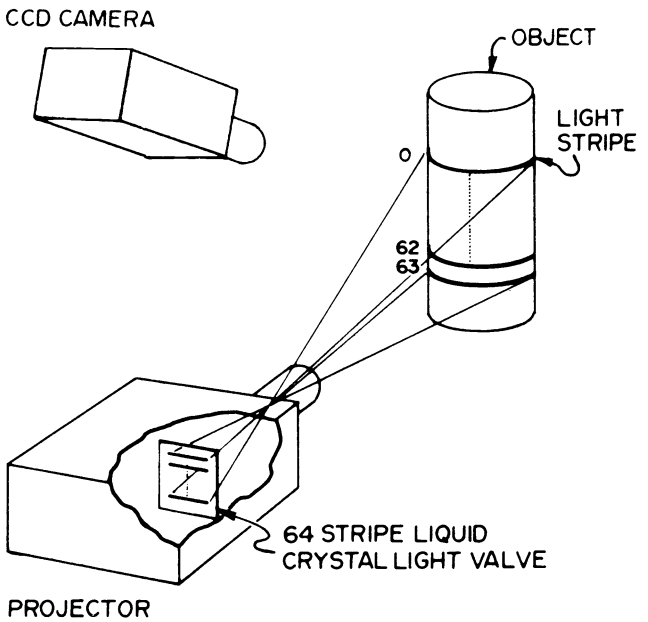

Fig. 1. Shape measurement system arrangement for which the centroid method is used to achieve subpixel accuracy in light stripe location.

jecting a sequence of stripe patterns using the liquid crystal. In each pattern the intensity of each light stripe indicates one bit in its code.

The light stripes are initially located in an image taken with all 64 stripes turned on. Since the light stripes are oriented approximately horizontally in the camera's image they can be located by searching for intensity peaks along each column of pixels. The intensity peak corresponding to each light stripe is delineated by a local minimum in intensity on either side. The center of the peak is estimated by the centroid of the area between the two minima and above a threshold level. This threshold level is either the intensity of the higher intensity minimum or a specified level T_c, whichever is greater. Level T_c is set just above the noise level and comes into use for isolated stripes or stripes on the edge of the array.

Let the intensity of the i'th pixel in a column of pixels be g_i. Let h_i equal g_i minus the threshold level with any resulting negative values of h_i set to zero. The stripe center $\bar{x}$ is calculated as the centroid of h_i between pixels m and n, the positions of the minima either side of the stripe:

$$\bar{x} = \frac{\sum_{i=m}^{n} i h_i}{\sum_{i=m}^{n} h_i} \quad . \tag{1}$$

3. SYSTEMATIC ERROR IN LIGHT STRIPE LOCATION USING THE CENTROID

Figure 2 illustrates the process of forming a sampled image of a single light stripe. (For simplicity of discussion we assume there is no ambient lighting.) Waveform $e(x)$ of Fig. 2(a) is the intensity profile of the image of the stripe on the surface of the CCD. Waveform $e(x)$ results from the convolution of $a(x)$, the ideal profile, with the line spread functions of the projector and camera lenses. Waveform $e(x)$ is convolved with $p(x)$ of Fig. 2(b), the pixel sensitivity profile, giving waveform $f(x)$ of Fig. 2(c). Then $f(x)$ is multiplied by the sampling function $s(x)$ (Fig. 2[d]) giving $g(x)$, the sequence of sample values, in Fig. 2(e).

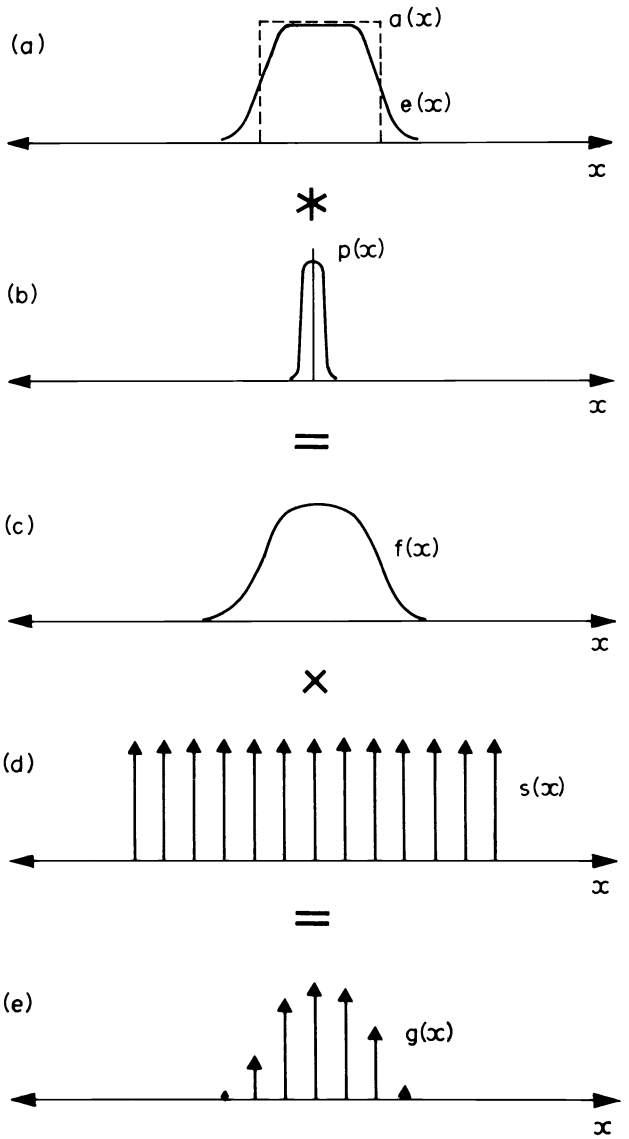

Fig. 2. The process of sampling an image of a projected stripe. (a) intensity profile $e(x)$ of light incident on the CCD surface [ideal profile $a(x)$ shown dotted]. (b) Pixel sensitivity profile $p(x)$. (c) Waveform $f(x)$ resulting from convolution of pixel sensitivity profile with stripe image intensity profile. (d) Sampling function $s(x)$. (e) Sample waveform $g(x)$ obtained by multiplying sampling function by $f(x)$.

If the pixel sensitivity profile is symmetrical it is clear that the centroid of waveform $f(x)$, given by

$$\overline{x_f} = \frac{\int_{-\infty}^{\infty} x f(x)\, dx}{\int_{-\infty}^{\infty} f(x)\, dx} \quad , \tag{2}$$

is equal to the centroid of $e(x)$.

The sample values g_i in the digitized image correspond to the impulses in waveform $g(x)$. The centroid of g_i, given by

$$\overline{x_g} = \frac{\sum_{i=-\infty}^{i=\infty} i g_i}{\sum_{i=-\infty}^{i=\infty} g_i} \quad , \tag{3}$$

is therefore equal to the centroid of $g(x)$

$$\overline{x_g} = \frac{\int_{-\infty}^{\infty} xg(x)\,dx}{\int_{-\infty}^{\infty} g(x)\,dx} . \tag{4}$$

As stated in Sec. 2, in practice the position of the stripe center is estimated by calculating the centroid of g_i between the minimum on each side of the stripe after subtraction of a threshold value. In evaluating the accuracy of this technique two aspects are considered in the following sections.

1. The relationship between the centroid of the continuous profile $f(x)$ and the centroid of the corresponding sampled intensity profile $g(x)$, for the ideal case of an isolated stripe and no noise. Systematic error will be present if the centroid of $g(x)$ is not equal to the centroid of $f(x)$.
2. The effect on accuracy of the practical situation of calculation of the centroid over a limited range of pixels after subtraction of a threshold.

The main aspect considered in this paper is the first above. The second is only briefly dealt with here.

3.1. Relationship between the centroids of continuous and sampled waveforms

The relationship between the centroid of a continuous function and its sampled equivalent can be well understood by considering the Fourier transforms of the two waveforms. Figure 3 shows, on the left, waveforms corresponding to Figs. 2(c), 2(d), and 2(e), and on the right, their Fourier transforms.[14] Since $f(x)$ is, in general, not an even function its transform, $F(s)$ has an imaginary part, which is shown dotted. Due to the various factors that cause blurring of the stripe, $F(s)$ will decrease for higher spatial frequencies and is zero above a cutoff frequency s_c.

Multiplication of $f(x)$ by the sampling function $s(x)$ gives the sampled function $g(x)$. Correspondingly, convolution of the Fourier transforms, $F(s)$ and $S(s)$, yields the Fourier transform $G(s)$ of Fig. 3(f), in which the transform of $f(x)$ is replicated at intervals of $1/T$, the sampling frequency (1 sample per unit distance in Fig. 3).

The centroid $\overline{x_f}$ of $f(x)$ is related to its Fourier transform as follows:[14]

$$\overline{x_f} = \frac{\int_{-\infty}^{\infty} xf(x)\,dx}{\int_{-\infty}^{\infty} f(x)\,dx} = -\frac{F'(0)}{2\pi jF(0)} . \tag{5}$$

We can see that the centroid of $f(x)$ is dependent only on the behavior of $F(s)$ and $F'(s)$ at the origin. Likewise, the centroid of the sampled function $\overline{x_g}$ will depend only on the behavior of $G(s)$and $G'(s)$ at the origin:

$$\overline{x_g} = \frac{\int_{-\infty}^{\infty} xg(x)\,dx}{\int_{-\infty}^{\infty} g(x)\,dx} = -\frac{G'(0)}{2\pi jG(0)} . \tag{6}$$

Therefore, if

$$G(0) = F(0) , \tag{7}$$

and

$$G'(0) = F'(0) , \tag{8}$$

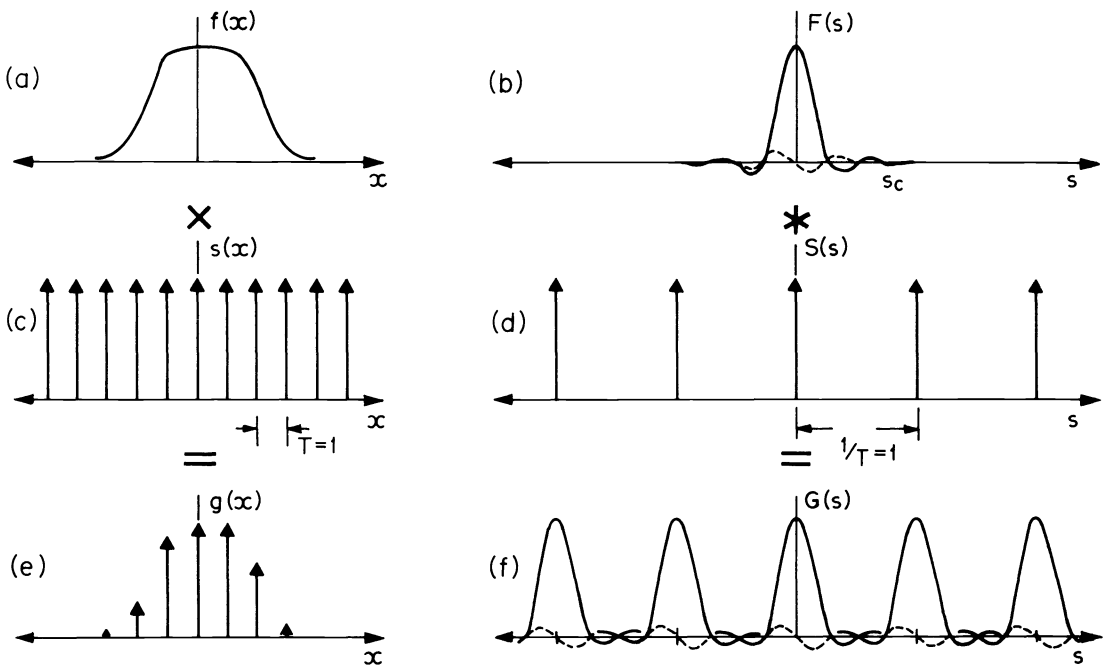

Fig. 3. Sampling in the spatial domain and the spatial frequency domain. (a) Intensity profile $f(x)$. (b) Fourier transform $F(s)$ of $f(x)$. (c) Sampling function $s(x)$. (d) Fourier transform of sampling function $S(s)$. (e) Waveform $g(x) = f(x)s(x)$. (f) Fourier transform of $g(x)$, $G(s) = F(s) * S(s)$.

then

$$\overline{x_g} = \overline{x_f} \ , \tag{9}$$

i.e., the centroid of the sampled function $g(x)$ will be equal to the centroid of the corresponding continuous function $f(x)$.

With reference to $G(s)$ in Fig. 3(f), it is apparent that Eqs. (7) and (8) will be satisfied if the replicated transforms of $f(x)$ do not overlap to such a degree that any part of a replicated transform is present at the origin. This will be the case if the cutoff frequency s_c is less than $1/T$, the sampling frequency, as shown.

Note that if the centroids of the sampled and continuous functions are to be equal, the critical cutoff frequency of $F(s)$ is the sampling frequency, not half the sampling frequency as is required for exact reconstruction of $f(x)$ from the sample values.

3.1.1. Two-dimensional centroid

An analogous analysis applies for the two-dimensional centroid. Given the two-dimensional Fourier transform $F(u,v)$ of a continuous function $f(x,y)$ the x and y values $(\bar{x},\bar{y})$ of the centroid of $f(x,y)$ are given[14] by

$$\bar{x} = \frac{\int_{-\infty}^{\infty}\int_{-\infty}^{\infty} xf(x,y)\,dx\,dy}{\int_{-\infty}^{\infty}\int_{-\infty}^{\infty} f(x,y)\,dx\,dy} = -\frac{F'_u(0,0)}{2\pi jF(0,0)} \ , \tag{10}$$

$$\bar{y} = \frac{\int_{-\infty}^{\infty}\int_{-\infty}^{\infty} yf(x,y)\,dx\,dy}{\int_{-\infty}^{\infty}\int_{-\infty}^{\infty} f(x,y)\,dx\,dy} = -\frac{F'_v(0,0)}{2\pi jF(0,0)} \ . \tag{11}$$

In analogy with the one-dimensional case, the centroid of $f(x,y)$ is dependent only on the behavior of $F(u,v)$ at the origin.

The Fourier transform of a sampled version $g(x,y)$ of $f(x,y)$ consists of replicated versions of $F(u,v)$ spread over the u,v plane at intervals of u and v equal to the sampling frequencies in the x and y directions, respectively. The centroid of $g(x,y)$ will be equal to the centroid of $f(x,y)$ if no part of any of the replicated versions of $F(u,v)$ is present at the origin. This will be the case if the cutoff frequency of $F(u,v)$ in the u direction is less than the x sampling frequency and the cutoff frequency in the v direction is less than the y sampling frequency.

3.2. Elimination of systematic error in practice

Given the above result, it is apparent that systematic error can be eliminated by a choice of camera lens aperture such that the lens MTF cutoff frequency due to diffraction lies below the sampling frequency. If the camera lens MTF cuts off at spatial frequency s_c, then $E(s)$ [the Fourier transform of $e(x)$], and hence $F(s)$, must cut off at s_c.

For incoherent light, the lens MTF cutoff frequency is $1/(\lambda F)$, where λ is the wavelength of light and F the lens f-number. The camera used for the experimental results presented later in this paper has a pixel pitch in the vertical direction of 13.5 μm giving a sampling frequency of 74.1 samples per mm. For λ equal to 550 nm (this value of λ will be used for all further calculations in this paper), a camera lens f-number greater than 24.5 will result in a cutoff frequency less than this sampling frequency and, consequently, no systematic error.

While this aperture of $f/24.5$ is small, it should be noted that wider apertures apply in the infrared.

3.3. Properties of the systematic error

If $F(s)$ does not cut off below the sampling frequency, systematic error will, in general, occur. It is of interest to calculate the properties of this error.

Let function $f_e(x)$ be even; its centroid is then zero. Let $f(x)$ equal $f_e(x)$ shifted by sampling offset d from the origin, i.e.,

$$f(x) = f_e(x - d) \ , \tag{12}$$

and

$$F(s) = \exp(-j2\pi ds)F_e(s) \ . \tag{13}$$

$G(s)$ consists of an infinite series of instances of $F(s)$,

$$\begin{aligned} G(s) &= \sum_{n=-\infty}^{\infty} F(s - n/T) \\ &= \sum_{n=-\infty}^{\infty} \exp[-j2\pi d(s-n/T)]\, F_e(s - n/T) \ . \end{aligned} \tag{14}$$

The centroid of $g(x)$ is a function of $G(0)$ and $G'(0)$. We have

$$\begin{aligned} G'(s) = \sum_{n=-\infty}^{\infty} \{&-j2\pi d \exp[-j2\pi d(s - n/T)]\, F_e(s - n/T) \\ &+ \exp[-j2\pi d(s - n/T)]\, F'_e(s - n/T)\} \ . \end{aligned} \tag{15}$$

Substituting $s = 0$ into Eqs. (14) and (15), and noting that $F_e(s)$ is even and $F'_e(s)$ is odd, gives

$$\begin{aligned} G(0) &= \sum_{n=-\infty}^{\infty} \exp(j2\pi dn/T)F_e(-n/T) \\ &= F_e(0) + \sum_{n=1}^{\infty} F_e(-n/T)\,[\exp(j2\pi dn/T) \\ &\quad + \exp(-j2\pi dn/T)] \\ &= F_e(0) + \sum_{n=1}^{\infty} F_e(n/T)2\cos 2\pi dn/T \ , \end{aligned} \tag{16}$$

and

$$\begin{aligned} G'(0) &= \sum_{n=-\infty}^{\infty} [-j2\pi d \exp(j2\pi dn/T)\, F_e(-n/T) \\ &\quad + \exp(j2\pi dn/T)\, F'_e(-n/T)] \\ &= -j2\pi dF_e(0) + \sum_{n=1}^{\infty} \{-j2\pi dF_e(-n/T) \\ &\quad \times [\exp(j2\pi dn/T) + \exp(-j2\pi dn/T)] \\ &\quad + F'_e(-n/T)\,[\exp(j2\pi dn/T) - \exp(-j2\pi dn/T)]\} \\ &= -j2\pi dF_e(0) + \sum_{n=1}^{\infty} [-j2\pi dF_e(n/T)2\cos 2\pi dn/T \\ &\quad - F'_e(n/T)2j\sin 2\pi dn/T] \ . \end{aligned} \tag{17}$$

Substituting Eqs. (16) and (17) into Eq. (6) to find the centroid of $g(x)$ gives

$$\overline{x_g} = \frac{-j2\pi dF_e(0) + \sum_{n=1}^{\infty}[-j2\pi dF_e(n/T)2\cos 2\pi dn/T - F'_e(n/T)2j\sin 2\pi dn/T]}{-2\pi j[F_e(0) + \sum_{n=1}^{\infty}F_e(n/T)2\cos 2\pi dn/T]}$$

$$= d + \frac{\sum_{n=1}^{\infty}F'_e(n/T)\sin 2\pi dn/T}{\pi[F_e(0) + \sum_{n=1}^{\infty}F_e(n/T)2\cos 2\pi dn/T]} . \quad (18)$$

Ideally the centroid of $g(x)$ would be d so the error δ is

$$\delta = \frac{\sum_{n=1}^{\infty}F'_e(n/T)\sin 2\pi dn/T}{\pi[F_e(0) + \sum_{n=1}^{\infty}F_e(n/T)2\cos 2\pi dn/T]} . \quad (19)$$

Consider the situation where the camera lens aperture is such that the MTF cutoff frequency is between $1/T$ and $2/T$. In this case δ simplifies to

$$\delta = \frac{F'_e(1/T)\sin 2\pi d/T}{\pi[F_e(0) + F_e(1/T)2\cos 2\pi d/T]} . \quad (20)$$

Generally $F_e(0)$ is much larger than $F_e(1/T)$ so the cosine term in the denominator can be ignored, giving

$$\delta \approx \frac{F'_e(1/T)\sin 2\pi d/T}{\pi F_e(0)} . \quad (21)$$

Therefore δ has the form $\sin\theta$ with θ ranging from $-\pi$ to π as the offset d is changed from -0.5 to 0.5 (for $T = 1$). The magnitude of δ is directly proportional to the slope of $F_e(s)$ at the sampling frequency.

The following points can be made:

- As noted by many authors,[7–10] increased blur will reduce systematic error. The preceding analysis has shown that the error will be reduced if the slope of $F_e(s)$ at the sampling frequency is reduced. This will occur for increasing degrees of blur in general. [Introduction of blur by use of a lens with large aberrations would, of course, not normally be useful. Blur due to aberrations is generally asymmetrical so the centroid of the intensity profile $e(x)$ of the light incident on the surface of the CCD would not correspond to the centroid of the ideal profile $a(x)$.]
- If the form of the image $e(x)$ incident on the image sensor's surface is relatively fixed (as would be the case when viewing a point source with a diffraction limited lens, for example) then the form of $f_e(x)$ and hence, $F_e(s)$, is fixed so the systematic error is predictable and can be corrected for. However, if the image varies significantly in size, as for example do the images of the projected light stripes used in the shape measurement system, the form of $F_e(s)$ will vary and the behavior of the systematic error will consequently vary. In this case, a correction for systematic error is not readily possible.

4. SIMULATIONS

This section describes the use of a simulation to investigate the predictions of the previous sections. The procedure used to evaluate the systematic error is direct calculation of the shape of waveform $f(x)$ for a particular optical arrangement. Then $f(x)$ is sampled and the centroid of the samples calculated and compared with the known centroid of $f(x)$. In order to simplify this process, $a(x)$ is made periodic and even. Each stripe is of amplitude 1, width W, and the stripe pitch is X. The case of an isolated stripe can be reasonably accurately handled by setting X to a relatively large value.

Note that the systematic error can be calculated directly using Eq. (19). However, the approach used here also allows the effect of calculation of the centroid over a limited range of pixels to be conveniently evaluated.

Since $a(x)$ is even, it is represented by the Fourier cosine series:[15]

$$a(x) = a_0 + \sum_{n=1}^{\infty} a_n \cos\frac{2n\pi}{X}x = \frac{W}{X} + \sum_{n=1}^{\infty}\frac{2}{n\pi}\sin\frac{Wn\pi}{X}\cos\frac{2n\pi}{X}x . \quad (22)$$

Given $a(x)$, $f(x)$ can be obtained by multiplying each coefficient a_n by the values of the modulation transfer functions of the camera lens, $M_c(s)$, and the CCD, $M_{ccd}(s)$, at frequency n/X. The reason for not considering the projector lens is given later.

$$f(x) = \frac{W}{X} + \sum_{n=1}^{\infty} M_c\left(\frac{n}{X}\right) M_{ccd}\left(\frac{n}{X}\right)\frac{2}{n\pi}\sin\frac{Wn\pi}{X}\cos\frac{2n\pi}{X}x . \quad (23)$$

As defined above, $f(x)$ is centered on the origin. The sequence of sample values g_i is generated by calculating the value of $f(x)$ at increments of 1 pixel along the x axis with the series of samples starting at sampling offset d from the origin, i.e.,

$$g_i = f[(i + d)T] . \quad (24)$$

Here d has units of pixel pitch. Varying d over the range -0.5 to 0.5 allows us to simulate the effect of moving the stripe relative to the array of pixels. The more natural approach would be to sample at $x = iT$ and move $f(x)$, but the technique used is more straightforward to implement. [Note that the sample values obtained using offset d above are equivalent to those obtained when sampling at $x = iT$ after shifting $f(x)$ by $-d$ from the origin.]

Given g_i, h_i is formed as described in Sec. 2. The centroid of h_i, given in pixel units by

$$\overline{x_h} = \frac{\sum_{i=m}^{i=n}(i + d)h_i}{\sum_{i=m}^{i=n}h_i} \quad (25)$$

would ideally equal the centroid of $f(x)$ (i.e.,zero) for any d. The systematic centroid error is $\overline{x_h} - 0 = \overline{x_h}$.

4.1. Modulation transfer functions

4.1.1. Lens MTF

The camera lens modulation transfer function for diffraction is

$$M_c(s) = \frac{2}{\pi}\{\cos^{-1}(\lambda Fs) - \lambda Fs\sin[\cos^{-1}(\lambda Fs)]\} \quad (26)$$

for points on the optical axis.[16] Here $M_c(s)$ cuts off at $s = 1/\lambda F$. For typical lenses this function should be reasonably accurate for apertures smaller than about $f/11$.

We do not consider the effect of the projector lens in the simulation because the height of the projector's image (the stripe array on the liquid crystal) is about four times that of the camera's image sensor. Consequently, given the same f-numbers for the two lenses, the effect of diffraction due to the camera lens will swamp that due to the projector lens if the projected stripe array fills the camera's image.

4.1.2. Image sensor MTF

The pixel sensitivity profile of width w can be approximated by

$$p(x) = \begin{cases} 0 & \text{when } x < -w/2 \\ 1/w & \text{when } -w/2 < x < w/2 \\ 0 & \text{when } x > w/2 \end{cases} . \tag{27}$$

The Fourier transform of $p(x)$ is

$$M_{\text{ccd}}(s) = \frac{\sin(w\pi s)}{w\pi s} . \tag{28}$$

Except where stated, the simulation results that follow apply to the camera used for the experimental measurements of centroid error presented in Sec. 5.1. This camera has an interline transfer CCD with a pixel pitch of 13.5 μm in the vertical direction. Clock electrodes separate the sensing elements and their width w in the vertical direction is approximately 10 μm.

Above, $p(x)$ applies for interline transfer CCDs used in the frame-integration mode in which charge is integrated for a whole frame period for each sensing element and alternate rows of sensing elements are read out for each field. Many interline transfer cameras use the field-integration mode in which all of the sensing elements are read out for each field but combined differently in alternate fields (e.g., elements in rows 1 and 2 would be combined to give the first line of the odd field and rows 2 and 3 combined for the first line of the even field). The pixel sensitivity profile for this mode consists of two instances of $p(x)$ spaced 1 pixel apart.

Finding the centroid using this sensitivity profile is equivalent to finding the centroid of sequence $k_i = g_i + g_{i+1}$, where g_i is the pixel intensity resulting using sensitivity profile $p(x)$. (Note that the sampling offset for k_i is shifted by 0.5 from that for g_i.) Here k_i is the result of convolving g_i with the sequence $m_i = \{1\ 1\}$. The centroid of a sequence resulting from the convolution of two sequences is the sum of the centroids of each of the sequences.[14] Consequently, the error in the centroid of k_i is equal to that in the centroid of g_i (after allowing for the sampling offset shift of 0.5). In summary, the centroid error for the field-integration mode has the same magnitude as that for the frame-integration mode.

4.2. Error versus lens aperture

First we evaluate the effect on the systematic error of varying the camera lens aperture. A stripe width of 3.85 pixels and stripe pitch of 32 pixels are used. The reason we use this stripe width is given later. We set T_c to zero so the centroid is evaluated over the range of pixels between and including the minimum on each side of the stripe. In this case, this range is 32 pixels. In practice, the centroid would not generally be evaluated over such a wide range due to the effect of noise.

For generality, we state the results in this section for lens f-numbers given as the ratio of the f-number used in the simulation F to the critical f-number F_c, such that the lens MTF cuts off exactly at the sampling frequency. The results can therefore be applied directly for any pixel pitch and wavelength of light.

Figure 4(a) shows $f(x)$ and the sample values when the sampling offset d is equal to 0.25 pixels and the camera lens f-number is half F_c. Figure 4(c) shows $f(x)$ and the sample values for a camera lens f-number just greater than $F_c (F/F_c = 1.02)$. The sampling offset is again 0.25 pixels. We observe the expected broadening of the edges of $f(x)$ for the smaller aperture due to the wider line spread function of the camera lens.

Figures 4(b) and 4(d) show the systematic error versus d for F/F_c equal to 0.5 and 1.02, respectively. (Note the change in scale of the vertical axis.) As expected, the error is considerably larger for $F/F_c = 0.5$ than for $F/F_c = 1.02$. The maximum errors are 0.043 pixel and 1.5×10^{-4} pixel, respectively. The form of the error curve in Fig. 4(b) is as expected from the analysis in Sec. 3.3. With $F/F_c = 0.5$ the MTF cut-off frequency is $2/T$ so the simplified result given in Eq. (21) applies. We expect the error to be an approximately sinusoidal function of the sampling offset, as is observed.

The error should ideally be zero for f-numbers greater than F_c. The residual error experienced here for the case $F/F_c = 1.02$ is due to evaluating the centroid over a range of only 32 pixels.

Figures 5(a) and 5(c) show $f(x)$ and the sample values for an input approximating an impulse. This was done by using a stripe width of 0.05 pixels. Figure 5(a) is for $F/F_c = 0.5$ and Fig. 5(c) for $F/F_c = 1.02$, d is equal to 0.25 for both figures. The intensity profile for $F/F_c = 1.02$ is appreciably wider than for $F/F_c = 0.5$, as expected. Note that the magnitude of $f(x)$ is small because the amplitude of the input $a(x)$ was one unit.

Figures 5(b) and 5(d) show the systematic error versus d for this stripe width. The systematic error is observed to be quite high for $F/F_c = 0.5$ with a maximum value of 0.19 pixel. The error decreases significantly for $F/F_c = 1.02$, as expected, with a maximum then of 1.5×10^{-3} pixel.

The error is expected to be larger in general for thinner stripes because the magnitude of $F_e(s)$, and hence its slope, will generally then be higher at the sampling frequency and its multiples. The form of the error curve for $F/F_c = 0.5$ of Fig. 5(b) differs slightly from a sinusoid because of the contribution of the cosine term in the denominator of Eq. (20), which was ignored when simplifying to the form of Eq. (21). This term is more significant in this case than for a width of 3.85 pixels because the magnitude of $F_e(s)$ is greater at the sampling frequency.

4.3. Variation of stripe width

In this and the following sections, we plot the systematic error for a range of stripe widths. First, in this section, we again consider the effect of varying the lens aperture.

In these simulations, we calculated the systematic error for stripe widths over the range 0.05 to 5.0 pixels with the sampling offset varied in steps of 0.05 pixel from 0.0 to 0.5 pixels for each width. We plotted the absolute value of the worst case error for each stripe width.

Figure 6 shows curves for three camera lens apertures, $F/F_c = 0.25$, $F/F_c = 0.5$, and $F/F_c = 1.02$. The reduction of error

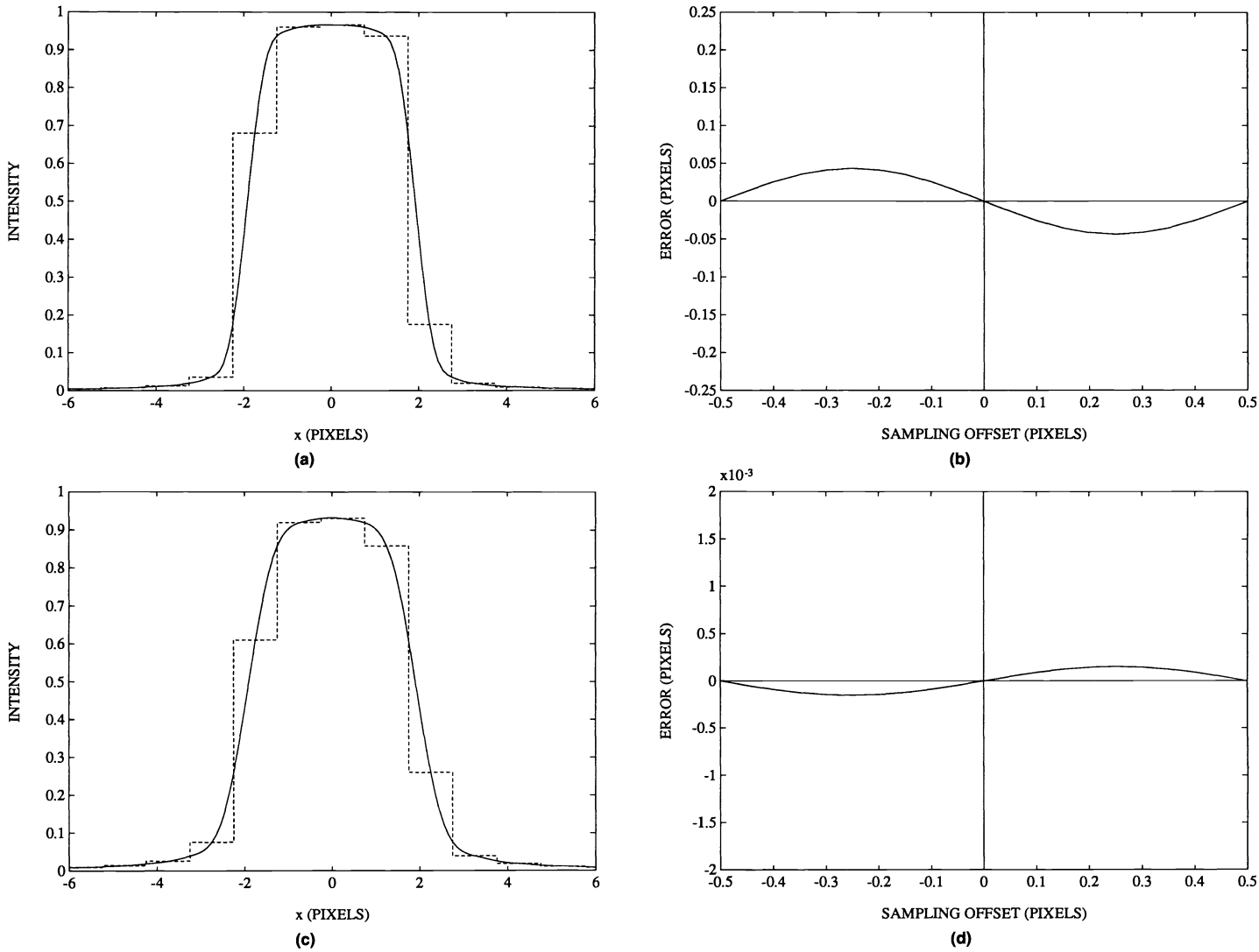

Fig. 4. Calculated stripe intensity profiles and systematic error for a stripe width of 3.85 pixels. (a) Intensity profile for $F/F_c = 0.5$. (b) Centroid error for $F/F_c = 0.5$. (c) Intensity profile for $F/F_c = 1.02$ (d) Centroid error for $F/F_c = 1.02$.

with increasing f-number is apparent. An overall reduction of error with increasing stripe width is also apparent.

The relationship between the systematic error and the stripe width is periodic. For $F/F_c = 0.5$ a local maximum occurs for a width of about 3.85 pixels, hence the use of this width in the examples of the previous section. This periodic relationship is explained shortly.

4.4. Comparison of sensor types

Figure 7 shows a comparison of systematic error for three sensor pixel sensitivity profile widths. The lens f-number was half F_c. Plots are given for sensitivity profile widths, in units of pixel pitch, of $w = 0.5$, $w = 0.74$, and $w = 1.0$.

The case $w = 0.74$ corresponds to the interline transfer CCD with pixel width of 10 μm and pitch of 13.5 μm, for which the previous simulations applied.

Frame transfer CCD sensors have no gaps between the sensitive areas of the pixels so $w = 1.0$ applies in this case. This curve also applies for frame transfer sensors that generate interlaced video output by accumulating the signal charge under different electrodes of each CCD stage during the integration time for each field. In this case, the sensitive areas of the pixels overlap and the pixel width is twice the pitch ($w = 2.0$). The sensitivity profile for $w = 2.0$ can be considered as two instances of profile $p(x)$ for $w = 1.0$ spaced one pixel apart. This profile was shown in Sec. 4.1.2 to give the same magnitude of systematic error as $p(x)$.

In these results, the systematic error is lower overall for wider sensitivity profiles. This trend does not continue indefinitely however. In Sec. 4.5.1 we show that systematic error is actually a periodic function of sensitivity profile width.

4.5. Form of the error versus stripe width relationship

The periodic variation in systematic error versus stripe width evident in the simulation results presented can be explained by considering the variation in the form of $F_e(s)$ versus stripe width. Here $F_e(s)$ is the product of $A_e(s)$, the Fourier transform of the ideal stripe intensity profile $a(x)$ when centered at the origin, the lens MTF $M_c(s)$, and the CCD MTF $M_{\text{ccd}}(s)$.

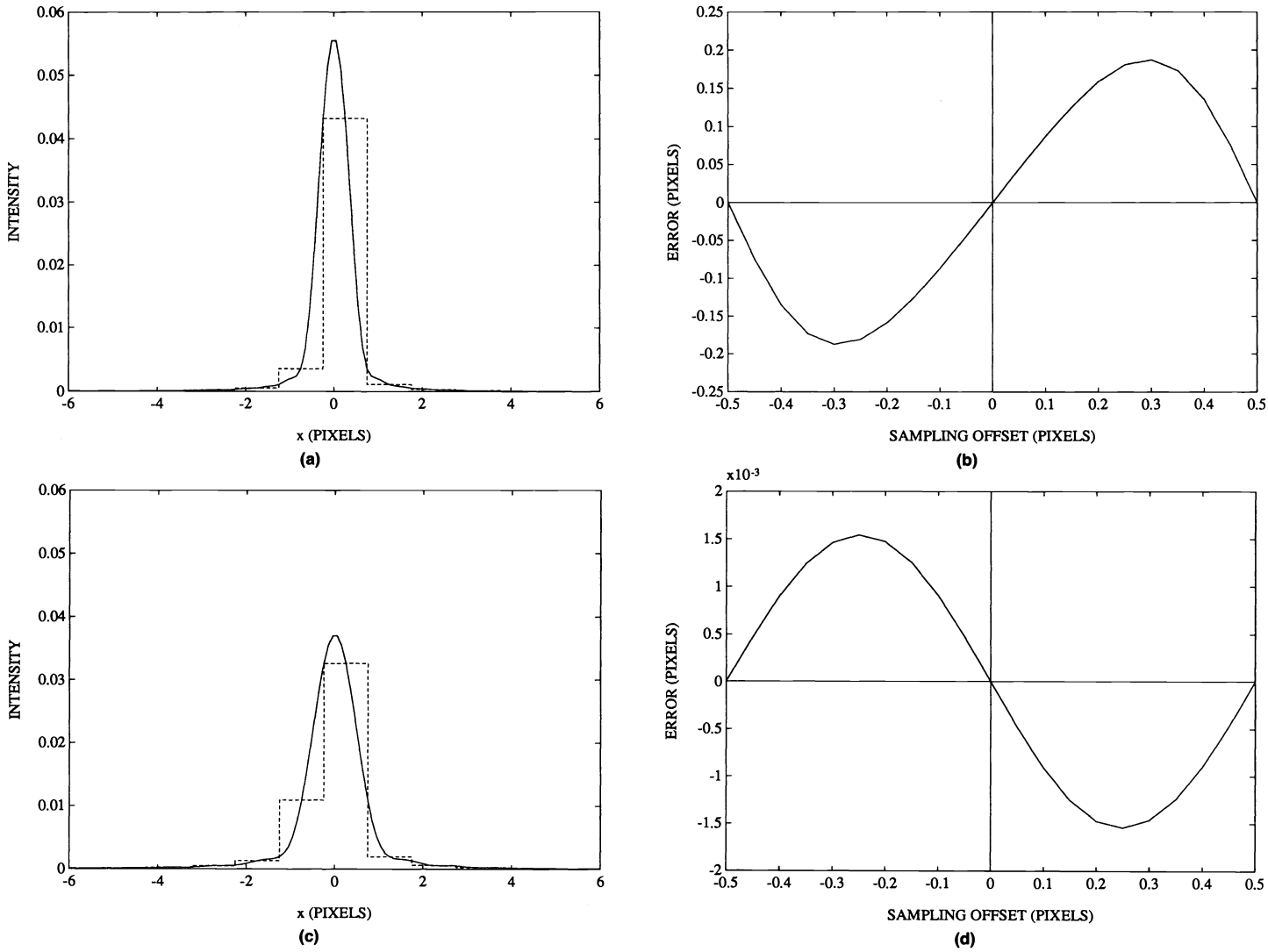

Fig. 5. Calculated stripe intensity profiles and systematic error for a stripe width of 0.05 pixels (approximates an impulse). (a) Intensity profile for $F/F_c = 0.5$. (b) Centroid error for $F/F_c = 0.5$. (c) Intensity profile for $F/F_c = 1.02$. (d) Centroid error for $F/F_c = 1.02$.

Given $a_e(x)$ for an isolated stripe defined as

$$a_e(x) = \begin{cases} 0 & \text{when } x < -W/2 \\ 1 & \text{when } -W/2 < x < W/2 \\ 0 & \text{when } x > W/2 \end{cases}, \tag{29}$$

then $A_e(s)$ is given by

$$A_e(s) = \frac{\sin(W\pi s)}{\pi s} . \tag{30}$$

$M_c(s)$ and $M_{ccd}(s)$ were defined earlier. Figure 8 shows $A_e(s)$, $M_c(s)$, $M_{ccd}(s)$, and $F_e(s)$ for $W = 2.0$, $F/F_c = 0.5$, and $w = 1.0$. The spatial frequency scale in this figure is normalized with respect to the sampling frequency. For display purposes, $A_e(s)$ and $F_e(s)$ have been scaled vertically by 0.5.

Consider the case of a stripe width of 1 pixel and a pixel sensitivity profile of width 1 pixel. Then $A_e(s)$ and $M_{ccd}(s)$ pass through zero at each integer multiple of the sampling frequency.

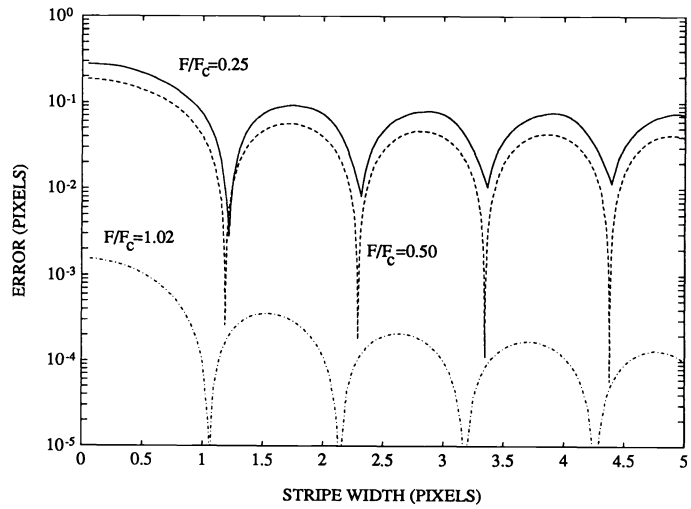

Fig. 6. Worst case systematic error versus stripe width and camera lens aperture.

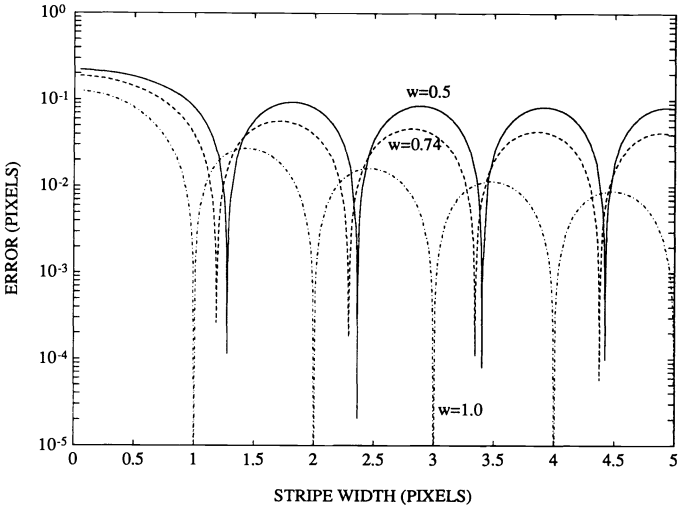

Fig. 7. Worst case systematic error versus stripe width for three CCD configurations (F/F_c = 0.5).

Both the slope and magnitude of $F_e(s)$ will therefore be zero at each multiple of the sampling frequency. The systematic error will therefore be zero, regardless of the lens f-number (see Eq. [19]). For wider stripe widths the zeros of $A_e(s)$ move toward the origin with a stripe width of 2 pixels resulting in the second zero crossing of $A_e(s)$ lying at the sampling frequency, as shown in Fig. 8. Systematic error will again be zero. At intermediate stripe widths the magnitude of $F_e(s)$ at multiples of the sampling frequency will still be zero, but the slope will not be zero so systematic error will be present. In summary, the error will be zero for integer stripe widths and nonzero otherwise. This behavior can be observed for the case $w = 1.0$ in Fig. 7.

The behavior for the other sensitivity profile widths in Fig. 7 are related to that for $w = 1.0$. Equation (19) shows that the systematic error is proportional to the slope of $F_e(s)$ at the sampling frequency. The minima in the curves for $w = 0.74$ and $w = 0.5$ occur for stripe widths such that the slope of $F_e(s)$ is zero at the sampling frequency. Ideally the error would be zero at these minima, but this is not the case here due to the effect of calculation of the centroid over a finite range of pixels.

Note that since $F/F_c = 0.5$ for Fig. 7, $F_e(s)$ cuts off at twice the sampling frequency so we need consider only the slope at the sampling frequency. For smaller values of F/F_c, we must also consider the slope at multiples of the sampling frequency. This explains the effect that the error at the minima of the curve for $F/F_c = 0.25$ in Fig. 6 does not decrease to as low a level as for $F/F_c = 0.5$. As for other f-numbers, these minima occur for stripe widths such that the slope of $F_e(s)$ at the sampling frequency is zero. However, the slope at $s = 2/T$ and $s = 3/T$ is not generally zero at these stripe widths so significant error still occurs. The error contributed by the second multiple of the sampling frequency will generally be the most significant. An error curve of the form sin2θ with θ ranging from $-\pi$ to π as d ranges from -0.5 to 0.5 is therefore expected. This effect has been observed under simulation.

4.5.1. Error versus pixel width relationship

Due to the similar forms of the pixel sensitivity profile $p(x)$ and the stripe profile $a_e(x)$, the plots of error versus stripe width for particular pixel sensitivity profile widths in Fig. 7 can equally apply as plots of error versus pixel width for particular stripe widths. For example, the error for a sensitivity profile width of 0.5 pixels and a stripe width of 1.0 pixels is equal to the error for a sensitivity profile width of 1.0 pixels and a stripe width of 0.5 pixels. When Fig. 7 is considered in this way, we see that given a particular stripe width the systematic error magnitude is a periodic function of sensitivity profile width. This result agrees with observations by Hegedus and Small[4] and could be of importance in scanning sensor applications where the pixel pitch can be flexibly varied.

4.6. Variation of threshold level

Figure 9 shows the effect of varying the threshold level T_c. All previous simulation results were for $T_c = 0.0$. Here T_c is specified as a fraction of the peak intensity of $f(x)$, $f(0)$. Curves for $T_c = 0.0$, $T_c = 0.01$, $T_c = 0.02$, and $T_c = 0.04$ are shown. All curves are for $F/F_c = 1.02$.

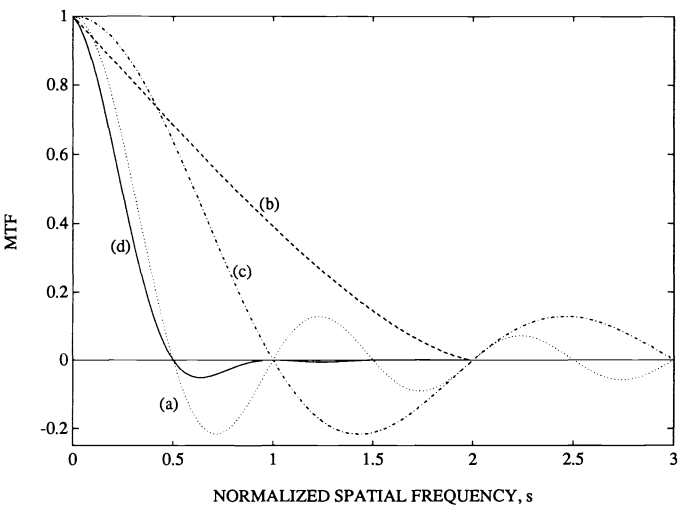

Fig. 8. Modulation transfer functions: (a) Fourier transform $A_e(s)$ of the ideal stripe intensity profile for a stripe width of 2 pixels. (b) Lens MTF curve $M_c(s)$ for $F/F_c = 0.5$. (c) CCD MTF $M_{ccd}(s)$ for a pixel sensitivity profile of width 1 pixel. (d) $F_e(s)$ resulting from the product of curves (a), (b), and (c).

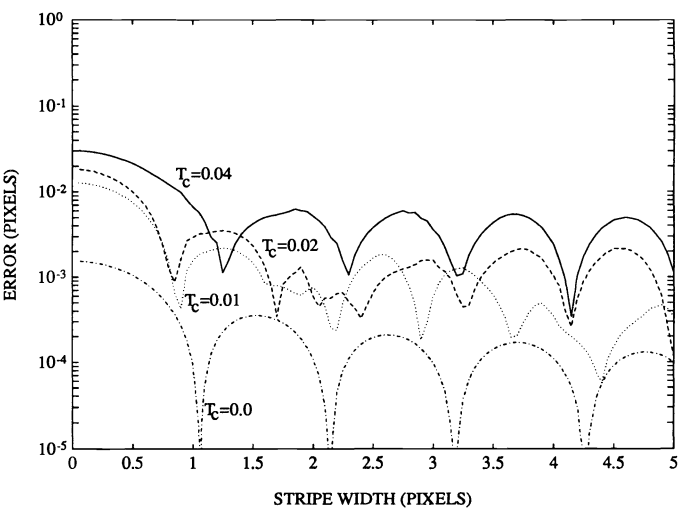

Fig. 9. Worst case systematic error versus stripe width for four threshold levels (F/F_c = 1.02).

For a stripe width of 0.05 pixels $T_c = 0.01$ results in either 6 or 7 pixels being used in the centroid calculation, depending on the sampling offset; $T_c = 0.02$ results in either 4 or 5 pixels; and $T_c = 0.04$ in either 3 or 4. The reduction of the number of pixels used in the centroid calculation by the use of higher threshold levels clearly introduces systematic error. In practice, this error must be traded off against error introduced due to noise, which increases as the number of pixels used in the centroid is increased.[8] A T_c below 0.04 is generally used in practice in the light stripe location application.

The above results apply for a pixel sensitivity profile width of 0.74 pixels. Figure 10 shows the effect of different profile widths for a particular threshold, $T_c = 0.04$. It is apparent that the error is smaller for the wider profiles. This is particularly so for a stripe width of 0.05 pixels.

Overall, the error introduced by practical threshold values is not large. It is clear, however, that in order to minimize error the threshold should be carefully chosen.

5. EXPERIMENTAL RESULTS

In order to measure the accuracy of light stripe center position estimation using the centroid we projected the array of stripes onto a flat surface. We evaluated centroid error by comparing the calculated center of a stripe using the centroid with an accurate estimate of the true center of the stripe for each of 100 columns of pixels. Since we knew the stripes to be straight in the image, we estimated the true center of the stripe by fitting a least-squares straight line to the series of center points found using the centroid.

We can readily detect systematic error in the calculated stripe center using this technique. The camera and projector are arranged such that the magnitude of the slope of the stripe in the image is small, so over the range of 100 pixels for which the centroid is calculated the stripe rises or falls by a few pixels. Since the slope is not zero the position of the stripe center relative to the rows of pixels (the sampling offset) is different for each column of pixels. If the difference between the calculated stripe center and the estimated true center is plotted against the column number, systematic error will be evident as a periodic waveform with period equal to the inverse of the stripe slope. Each period of this waveform is equivalent to a plot of the type shown in Fig. 4(b), where we plotted the systematic centroid error against the sampling offset.

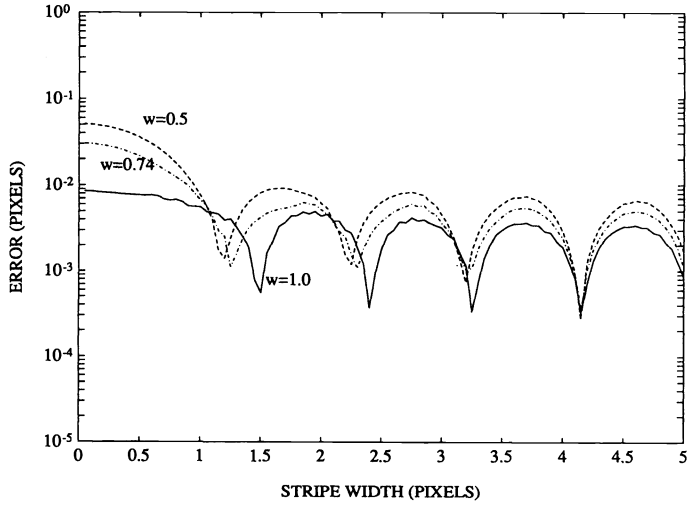

Fig. 10. Worst case systematic error versus stripe width for $T_c = 0.04$ and three pixel sensitivity profiles ($F/F_c = 1.02$).

The numerical measure of centroid error used is the standard deviation of the difference between the calculated stripe center and the estimated true center.

5.1. Experimental investigation of systematic centroid error

We measured the properties of the systematic error for a stripe width of approximately 4.0 pixels and with alternate stripes of the array turned on. With alternate stripes used, the gap between stripes is sufficient for the effect of the adjacent stripes to be insignificant. The stripe mark to space ratio is then 1:2.4.

We used an NEC model TI-22AII camera. This camera's image sensor is an interline transfer CCD with pixel pitch of 13.5 μm and sensitivity profile width of approximately 10 μm. The CCD was used in the frame integration mode. Images were digitized with eight-bit quantization using a Matrox MVP-AT video digitizer. A Micro-Nikkor 55 mm *f*/2.8 lens was used on the camera and a Schneider Companon-S 100 mm *f*/5.6 lens was used on the projector. An image with all stripes turned off was subtracted from the image with stripes on to remove ambient lighting effects. In order to reduce error due to random noise both images were generated by averaging 100 frames.

The optical configurations tested were:

1. Camera and projector lenses sharply focused and the camera lens aperture set to *f*/8. Assuming a mean wavelength of 550 nm the critical *f*-number for the camera used is *f*/24.5. Systematic error is therefore expected to be present.
2. Camera and projector lenses sharply focused and the camera lens aperture set to *f*/32. Since this *f*-number is greater than the critical *f*-number, systematic error should be reduced significantly in comparison with configuration 1.

We made no change in the experimental set up between each case and used the same 100 pixel segment of one particular stripe in both cases to allow direct comparison of the results. The average peak intensity of the stripes was slightly different for the two configurations. For configuration 1 it was 185 grey levels, for configuration 2, 181 grey levels. Threshold T_c was set to five grey levels for configuration 1 and eight grey levels for configuration 2. The ratio of T_c to the stripe peak intensity was therefore 0.027 and 0.044, respectively.

Figure 11(a) shows the results for configuration 1. Systematic error is clearly visible in the form of a periodic waveform. The slope of the stripe in the image was 0.067 so the period is expected to be 15 pixels, as can be observed. The standard deviation of the error was 0.033 pixels.

The amplitude of the error for a stripe width of four pixels, an *f*-number of *f*/8 and $T_c = 0.027$ was predicted to be 0.061 pixels by the simulation. This corresponds to a standard deviation of 0.043 pixels, assuming a sinusoidal error curve. The measured error is slightly lower than this estimate because of the effect of aberrations and the effect of the projector lens, which we ignored in the simulation.

Figure 11(b) shows the results for configuration 2. Significant differences can be seen between this plot and that of Fig. 11(a). No systematic error is evident. Any remaining systematic error is masked by error due to noise and deviations from straightness of the stripe. The standard deviation of the error was 0.013 pixels.

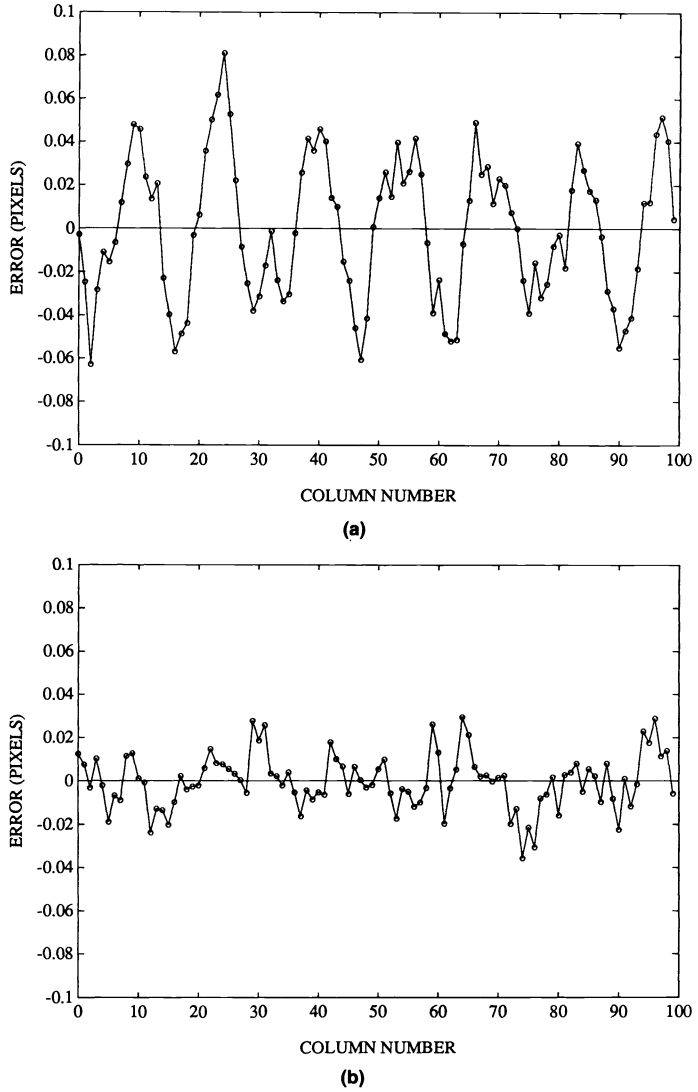

Fig. 11. Experimental results for systematic error for a stripe width of 4.0 pixels. (a) Camera and projector sharply focused, camera lens aperture *f*/8. (b) Camera and projector sharply focused, camera lens aperture *f*/32.

6. CONCLUSIONS

We have shown that the centroid of the digitized image of an image feature is free of systematic error if the maximum spatial frequency of the image incident on the sensor is less than the sampling frequency. In practice, this can be achieved by using a lens aperture such that the cut-off frequency due to diffraction is less than the sensor's sampling frequency. For the camera used here, this critical *f*-number is *f*/24.5.

In the situation where the lens *f*-number is lower than the critical *f*-number, systematic error is introduced. The use of a spatial-frequency-based approach in the analysis here has led to succinct explanations of many of the properties of this error. We applied these results in the case of the location of light stripes. Analysis showed that the error will vary approximately sinusoidally as the stripe is shifted over the sensing elements. This agrees with observation. We used simulation to evaluate the magnitude of the systematic error for a range of lens apertures, stripe widths, and pixel sensitivity profile forms. Error decreased, as expected, with higher *f*-numbers, becoming insignificant for *f*-numbers higher than the critical *f*-number. We observed a periodic relationship between error and stripe width with error being greatest for small stripe widths. Wider pixel sensitivity profiles were found to reduce error in general. However, we found the error to be a periodic function of sensitivity profile width.

We used simulation to judge the effect of the threshold used to limit the number of pixels used in the centroid calculation. We saw that the error introduced by practical threshold values is generally fairly small. Wider pixel sensitivity profiles were found to result in less error being introduced, given a particular threshold level.

Finally, experimental results support the prediction that systematic error is eliminated for lens *f*-numbers above the critical *f*-number.

7. ACKNOWLEDGMENT

This work has been supported by the Monash University Computer Centre Research and Development Fund.

8. REFERENCES

1. B. F. Alexander and K. C. Ng, "3-D shape measurement by active triangulation using an array of coded light stripes," in Optics, Illumination and Image Sensing for Machine Vision II, D. J. Svetkoff, ed., Proc. SPIE 850, 199–209 (1987).
2. B. F. Alexander, "High accuracy non-contact three dimensional shape measurement," Ph.D. thesis, Monash University (1989).
3. J. A. Jalkio, R. C. Kim, and S. K. Case, "Three dimensional inspection using multistripe structured light," *Opt. Eng.* 24(6), 966–974 (1985).
4. Z. S. Hegedus and G. W. Small, "Shape measurement in industry with sub-pixel definition," in Image Science '85, Acta Polytechnica Scandinavica Applied Physics Series, No. 150, 101–104 (1985).
5. Y. Takagi and S. Hata, "High speed precise 3-D vision sensor using slit-light method," in Proc. International Workshop on Industrial Applications of Machine Vision and Machine Intelligence, IEEE, 235–239 (1987).
6. P. Seitz, "Optical superresolution using solid-state cameras and digital signal processing," *Opt. Eng.* 27(7), 535–540 (1988).
7. E. P. Krotkov, "Visual hyperacuity: representation and computation of high precision position information," *Computer Vision, Graphics, and Image Processing* 33, 99–115 (1986).
8. S. B. Grossman and R. B. Emmons, "Performance analysis and size optimization of focal planes for point-source tracking algorithm applications," *Opt. Eng.* 23(2), 167–176 (1984).
9. J. A. Cox, "Evaluation of peak location algorithms with subpixel accuracy for mosaic focal planes," in Processing of Images and Data from Optical Sensors, W. H. Carter, ed., Proc. SPIE 292, 288–299 (1981).
10. J. A. Cox, "Advantages of hexagonal detectors and variable focus for point-source sensors," *Opt. Eng.* 28(11), 1145–1150 (1989).
11. R. H. Stanton, J. W. Alexander, E. W. Dennison, T. A. Glavitch, and L. F. Hovland, "Optical tracking using charge-coupled devices," *Opt. Eng.* 26(9), 930–938 (1987).
12. P. M. Salomon and T. A. Glavich, "Image signal processing in sub-pixel accuracy star trackers," in Smart Sensors II, D. F. Barbe, ed., Proc. SPIE 252, 64–74 (1980).
13. Y. Bar-Shalom, H. M. Shertukde, and K. R. Pattipati, "Use of measurements from an imaging sensor for precision target tracking," *IEEE Trans. Aerospace Electron. Sys.* 25(6), 863–872 (1989).
14. R. N. Bracewell, The Fourier Transform and Its Applications, second ed., McGraw-Hill, New York (1978).
15. E. Kreyszig, Advanced Engineering Mathematics, third ed., Wiley, New York (1972).
16. W. J. Smith, Modern Optical Engineering, McGraw-Hill, New York (1966).

Brian F. (Rick) Alexander received his B.Eng. and Ph.D. degrees from Monash University in 1983 and 1990, respectively. His Ph.D. work involved the development of a noncontact three-dimensional shape measurement system based on active triangulation. He is currently working at Monash University on the further development and application of this system. He has authored or coauthored seven papers in the area of noncontact three-dimensional measurement.

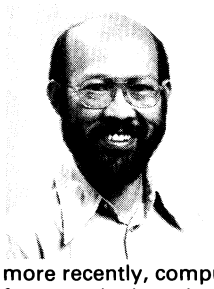

Kim Chew Ng obtained his Ph.D. degree from Queen's University, Belfast, in 1964. He was then appointed a National Physical Laboratory Research Fellow before joining the staff of the newly founded University of Warwick in 1965. In 1972 he moved to the University of Singapore and then to Monash University in 1975. His early research interest in adaptive control and automation has been supplanted over the years by electronics, instrumentation, circuit theory, biophysics, and more recently, computer vision. Besides papers in journals and conferences, he has also published a book on electrical network theory.